Supplementary Information

Modifying a Partial Corn-*sql* Layer-based (3,3,3,3,4,4)-c Topological MOF by Substitution of OH^- with Cl^- and its Highly Selective Adsorption of C2 Hydrocarbons over CH_4

Hongtao Cheng[a], Qian Wang*[a], Min Ding[a], Yajun Gao[b], Dongxu Xue[a] and Junfeng Bai*[a]

[a] *Key Laboratory of Applied Surface and Colloid Chemistry, Ministry of Education, School of Chemistry & Chemical Engineering, Shaanxi Normal University, Xi'an 710062, PR China*

[b] *State Key Laboratory of Coordination Chemistry, School of Chemistry & Chemical Engineering, Nanjing University, Nanjing 210093, PR China.*

General procedures. All reagents were obtained from commercial vendors and, unless otherwise noted, were used without further purification. Elemental analysis (C, H, N) were carried out with an Elementar Vario EL III. The IR spectra were obtained in the 4000~400 cm^{-1} on a Bruker Tensor27 spectrometer using KBr pellets. Thermal gravimetric analyses (TGA) were performed under N_2 atmosphere (100 ml/min) with a heating rate of 5 °C/min using a Beijing Henven HTG-1 thermogravimetric analyzer. Powder X-ray diffraction (PXRD) data were collected on a Bruker D8 ADVANCEX-ray diffractometer with Cu Kα radiation. The content of Cu and Li in MOF sample was carried out with Optima 5300 DV ICP.

X-ray crystallography. Single-crystal X-ray diffraction data were measured on a Bruker D8 Venture at 153 K using graphite monochromated Cu/Kα radiation (λ = 1.54178 Å). Data reduction was made with the Bruker SAINT program. The structures were solved by direct methods and refined with full-matrix least squares technique using the SHELXTL package[1]. Non-hydrogen atoms were refined with anisotropic displacement parameters during the final cycles. Organic hydrogen atoms were placed in calculated positions with isotropic displacement parameters set to 1.2 × U_{eq} of the attached atom. The unit cell includes a large region of disordered solvent molecules, which could not be modelled as discrete atomic sites. We employed PLATON/SQUEEZE[2] to calculate the diffraction contribution of the solvent molecules and, thereby, to produce a set of solvent-free diffraction intensities; structures were then refined

again using the data generated. A summary of the crystallographic data are given in Table S1. CCDC 1878404 contains the supplementary crystallographic data for SNNU-Bai67.

Table S1. Crystallographic Data of SNNU-Bai67

MOFs	**SNNU-Bai67**
Empirical formula	$C_{47}H_{43}Cl_2Cu_6N_9O_{25}$ [+4DMF·6(H_2O)]
Formula weight	1585.04
T [K]	153(2)
Wavelength [Å]	1.54178
Crystal system	Monoclinic
Space group	$P2_1$
a [Å]	14.9785(6)
b [Å]	18.7174(8)
c [Å]	15.2305(6)
α [deg]	90
β [deg]	102.450(2)
γ [deg]	90
V [$Å^3$]	4169.6(3)
Z	2
ρ_{calc}[g cm^{-3}]	1.263
μ [mm^{-1}]	2.816
F(000)	1592
Crystal size [mm^3]	0.13 × 0.1 × 0.08
Theta range [deg]	3.835 − 72.419
Limiting indices	-18 < = h < = 13
	-23 < = k < = 22
	-18 < = l < = 18
Reflections collected	32433
Reflections unique	14901 [R(int) = 0.0476]
Completeness	98.9 %
Data/restraints/parameters	14901 / 22 / 803
Goodness-of-fit on F^2	1.027
R1, wR2[a] [I>2σ(I)]	0.0409, 0.1186
R1, wR2[a][all data]	0.0416, 0.1198
$\Delta\rho_{max}$ / $\Delta\rho_{min}$[e. $Å^{-3}$]	-0.642 / 0.911

[a] $R1 = \Sigma||F_o| - |F_c||/|F_o|$; $wR2 = [\Sigma w(\Sigma F_o^2 - F_c^2)^2/\Sigma w(F_o^2)^2]^{1/2}$.

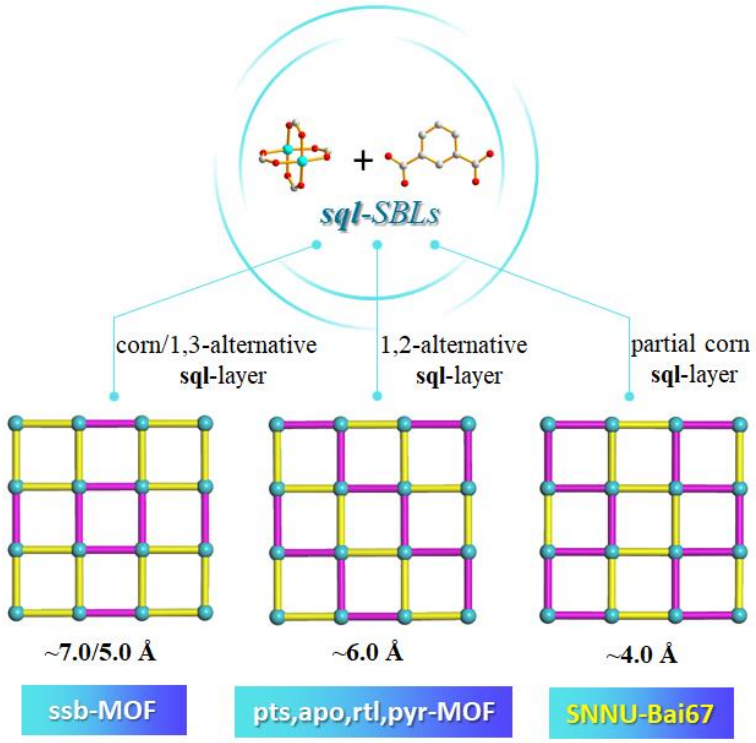

Figure S1. The illustrative graphics of three different kinds of *sql*-layers constructed by Cu-paddlewheel unit and isophthalate fragment exhibiting different pore sizes with the purple bond representing the 5-carbon atom in the isophthalate pointing "up" and the orange bond representing the 5-carbon atom in the isophthalate pointing "down", and the corresponding MOFs resulted from each *sql*-layer.

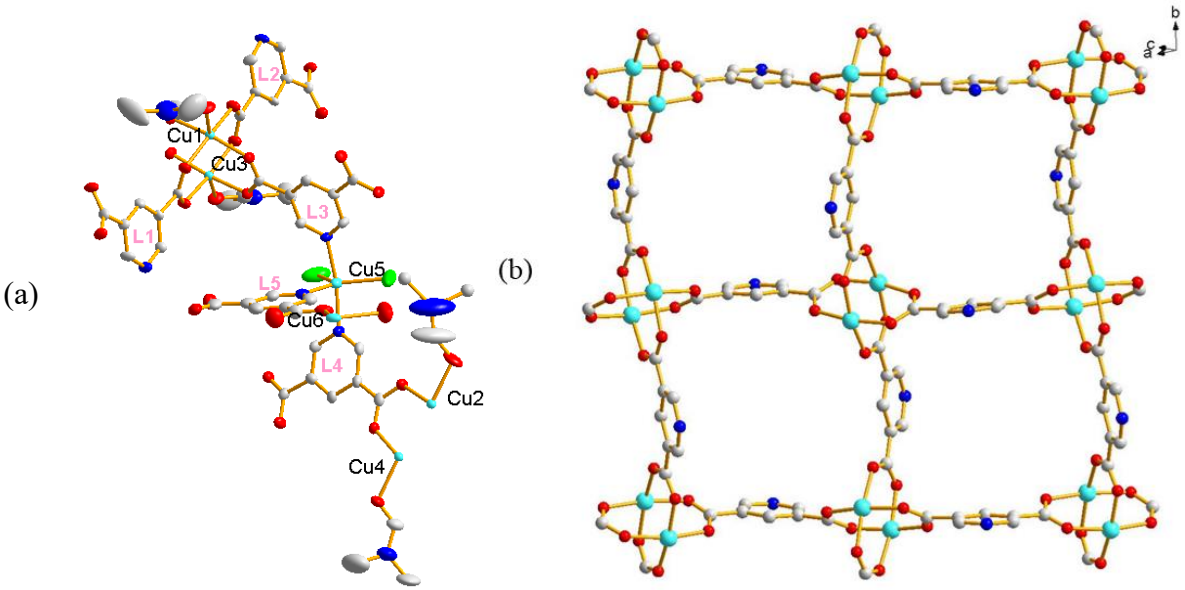

Figure S2. The asymmetric unit in the ellipsoid mode (a) and the partial corn-*sql* layer of SNNU-Bai67 (b). H atoms have been omitted for clarity.

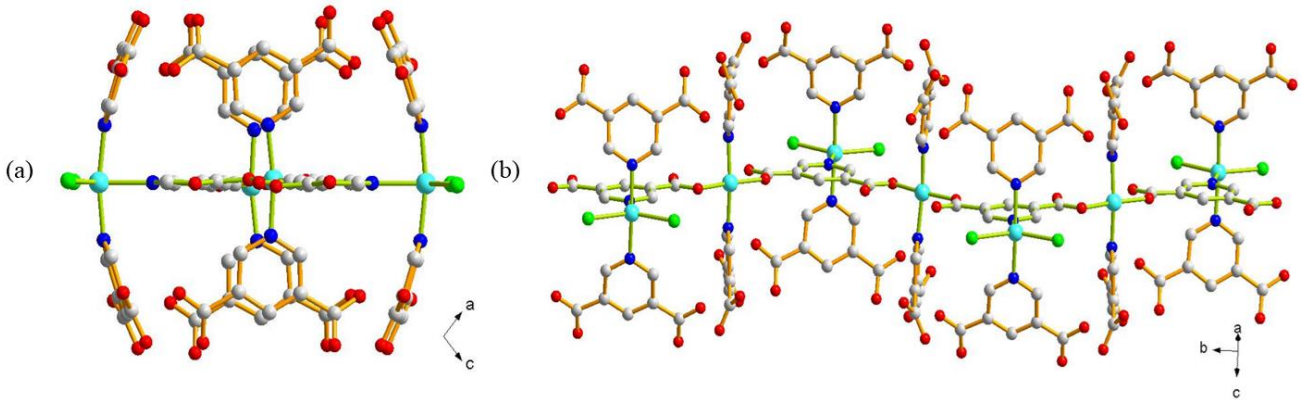

Figure S3. The chain of pillar viewed along (a) **b** axis and (b) (**a**+**c**) axis in SNNU-Bai67.

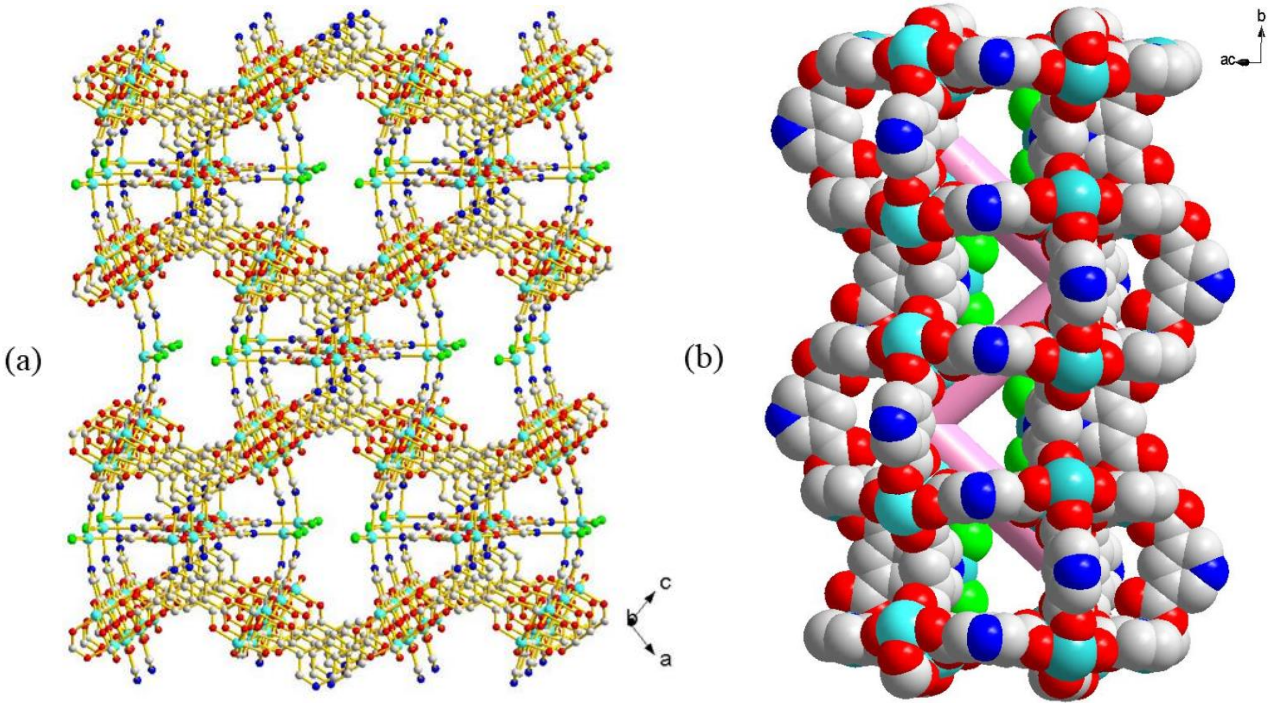

Figure S4. (a) The 3D structure viewed along **b** axis in SNNU-Bai67; (b) the 1D channel in SNNU-Bai67.

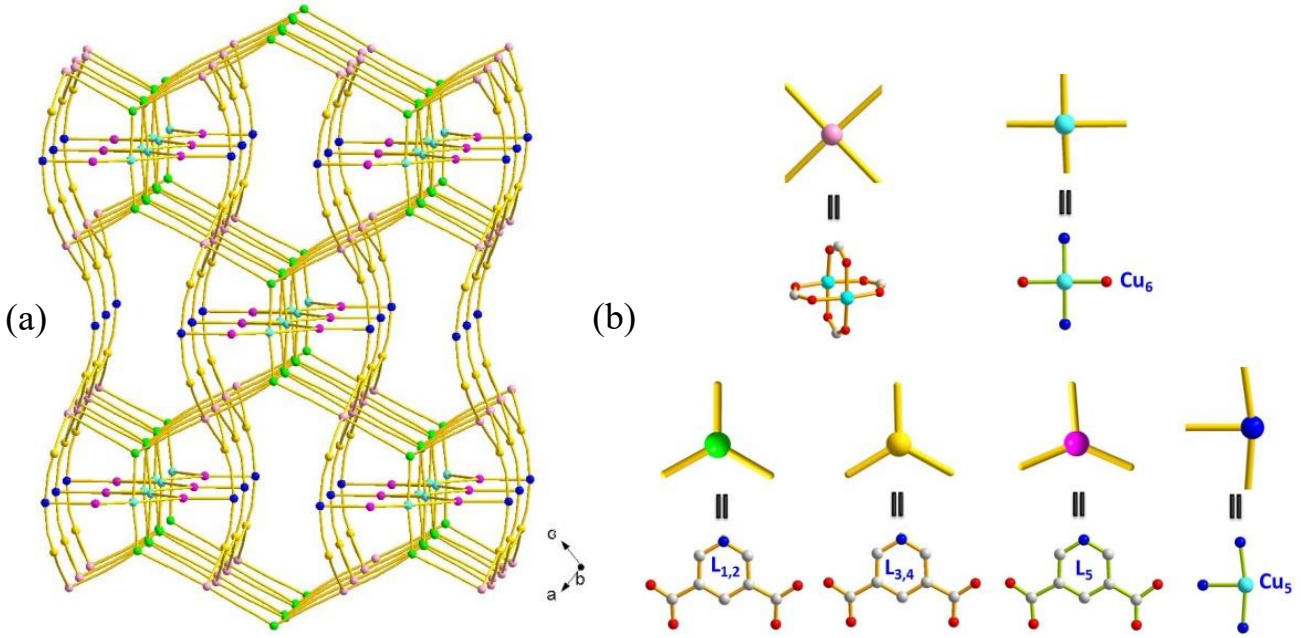

Figure S5. The 3D topological net with point symbol of $\{6^2.8^2.10.12\}_2\{6^2.8\}_6\{6^4.8.10\}$ viewed along **b** axis (a) and two kinds of 4-connected nodes and four different 3-connected nodes (b) in SNNU-Bai67.

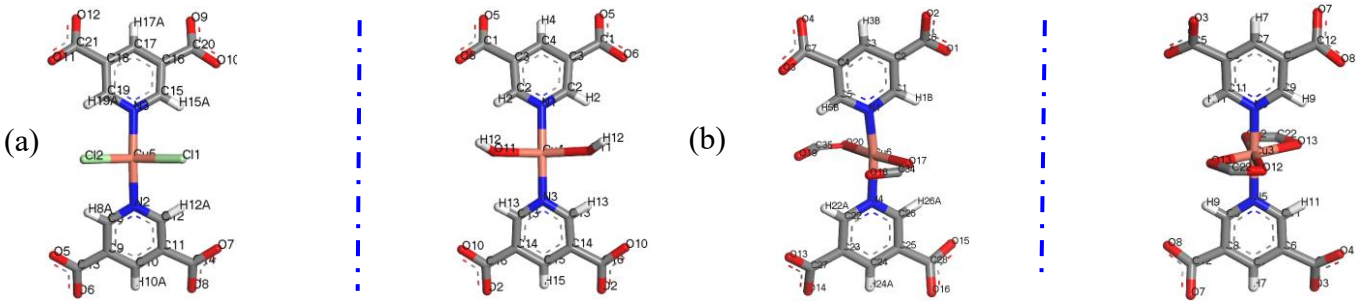

Figure S6. Comparisons of the coordination environments for two kinds of mononuclear Cu^{2+} ions in SNNU-Bai67 and VNU-18.

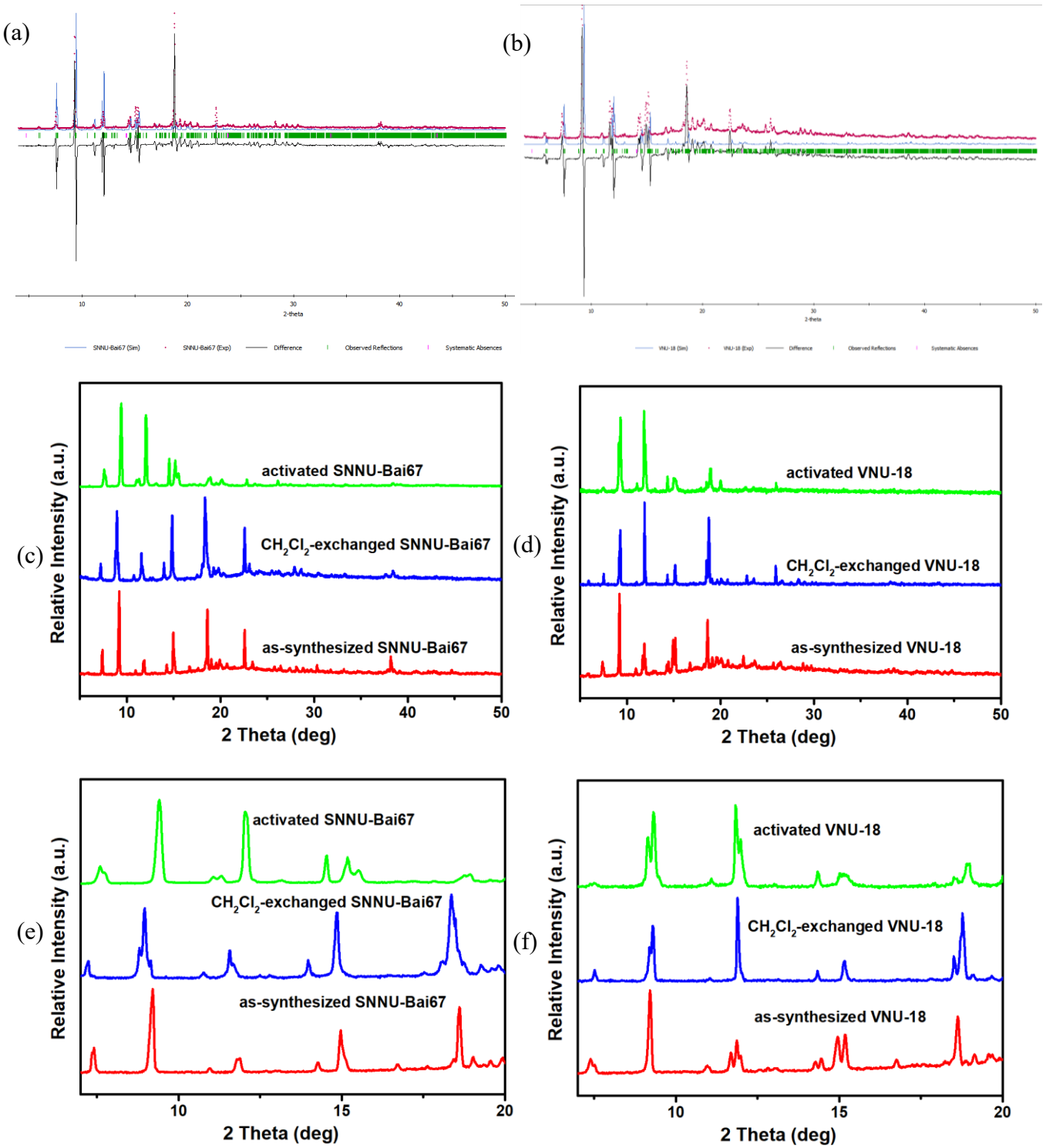

Figure S7. The simulated and experimental PXRD patterns and their differences of SNNU-Bai67 (a) and VNU-18 (b); PXRD patterns of as-synthesized, CH_2Cl_2-exchanged and activated SNNU-Bai67 (c) and VNU-18 (d); slight flexibility of SNNU-Bai67 (e) and VNU-18 (f) after CH_2Cl_2-exchange and activation.

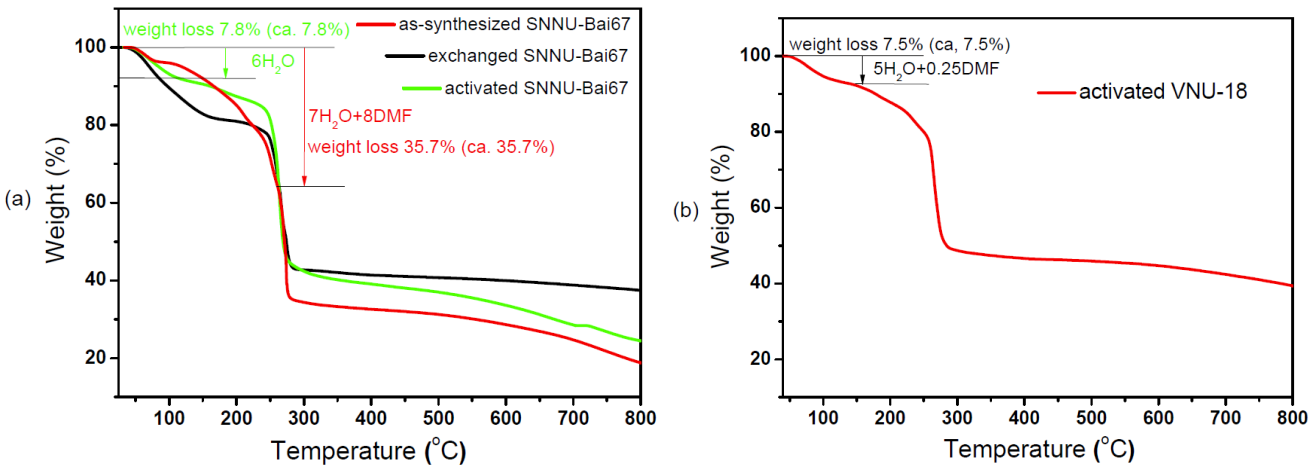

Figure S8. TGA curves of as-synthesized (red), CH_2Cl_2-exchanged (blue) and activated (green) SNNU-Bai67 (a) and VNU-18 (b).

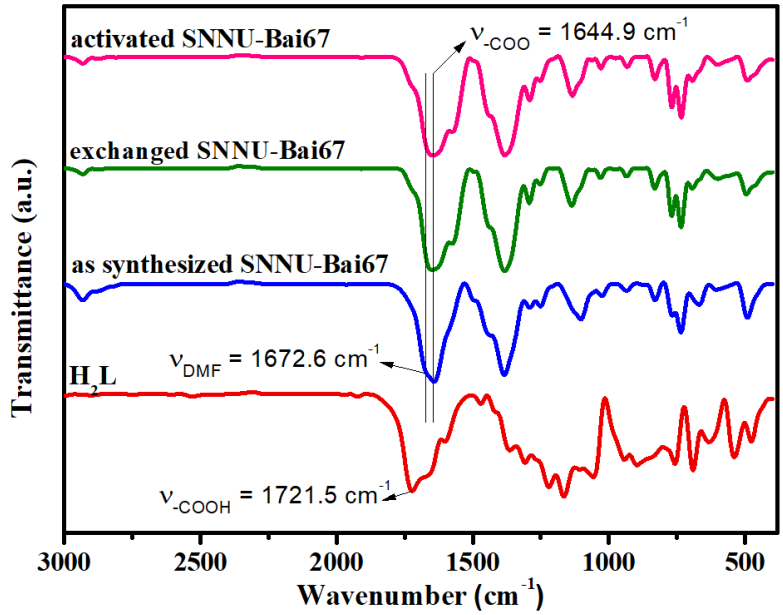

Figure S9. Infrared spectra of ligand (red), as-synthesized (blue), CH_2Cl_2-exchanged (green), and activated (pink) SNNU-Bai67. In the spectrum of H_2L, the IR peak of -COOH is evident at 1721.5 cm^{-1} and it shifted to 1644.9 cm^{-1} after its coordination with Cu^{2+} ion in as-synthesized, CH_2Cl_2-exchanged, and activated SNNU-Bai67. Moreover, in the spectrum of as-synthesized SNNU-Bai67, the IR peak of DMF molecule is evident at 1672.6 cm^{-1} and it disappeared after the CH_2Cl_2 exchanged into the pores of exchanged SNNU-Bai67 and in activated SNNU-Bai67, which indicated the successful CH_2Cl_2-exchange in exchanged SNNU-Bai67 and full activation of activated SNNU-Bai67.

Gas sorption measurements. Low-pressure adsorption isotherms of N_2 (99.999%), C_2H_2 (99.999%), C_2H_4 (99.999%), C_2H_6 (99.999%) and CH_4 (99.999%) gases were performed on Micromeritics 3Flex surface area and pore size analyzer. Before analysis, about 50 mg samples were activated by using the "outgas" function of the surface area analyzer. For all isotherms, ultra-high purity He gas (UHP grade 5.0, 99.999% purity) was used for the estimation of the free space (warm and cold), assuming that it is not adsorbed at any of the studied temperatures. The specific surface areas were determined using the Brunauer-Emmett-Teller (BET) and the Langmuir equation from the N_2 sorption data at 77 K. When applying the BET theory, we made sure that our analysis satisfied the two consistency criteria as detailed by Walton and co-workers.[3] For the Langmuir surface area, data from the whole adsorption data were used.

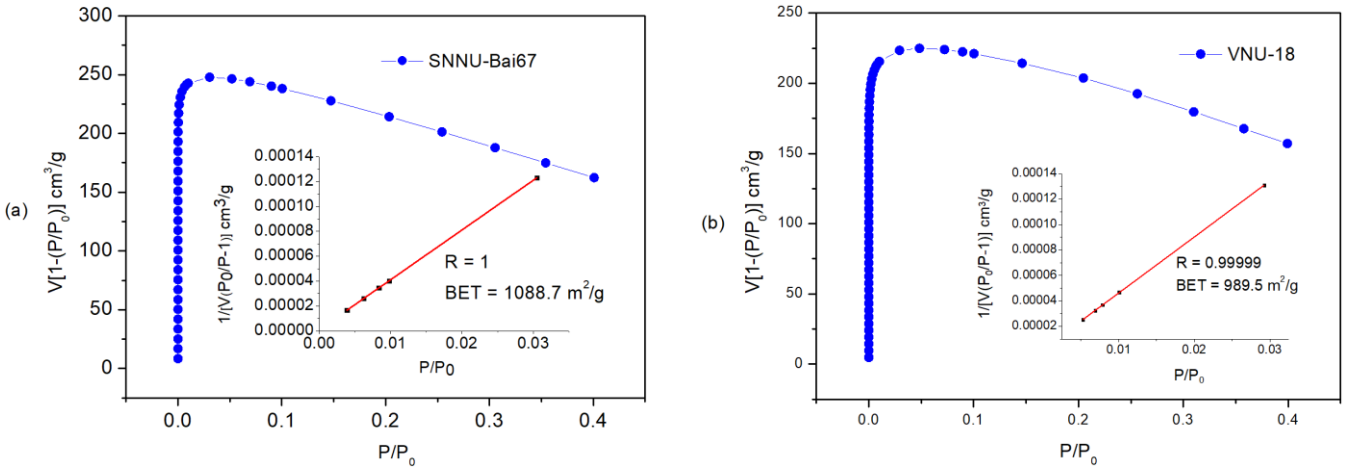

Figure S10. The $V[1-(P/P_0)]$ vs. P/P_0 for SNNU-Bai67 (a) and VNU-18 (b), only the range below P/P_0 = 0.04 or 0.03 satisfies the first consistency criterion for applying the BET theory. Inset: Plot of the linear region for the BET equation.

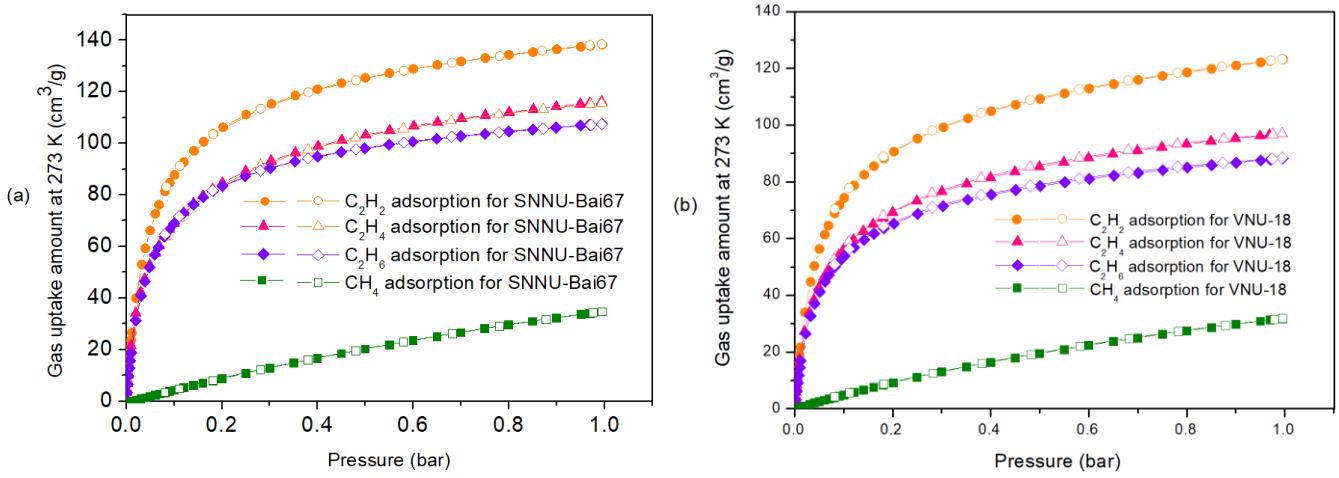

Figure S11. C_2H_2, C_2H_4, C_2H_6 and CH_4 adsorption isotherms for SNNU-Bai67 (a) and VNU-18 (b) at

273 K with the unit of gas uptake as cm^3/g (STP); Filled and open symbols represent adsorption and desorption, respectively.

Estimation of the isosteric heats of gas adsorption. A virial-type[4] expression comprising the temperature-independent parameters a_i and b_j was employed to calculate the enthalpies of adsorption for C_2H_2, C_2H_4, C_2H_6 and CH_4 (at 273 and 298 K) of activated SNNU-Bai67. In each case, the data were fitted using the equation:

$$\ln P = \ln N + 1/T \sum_{i=0}^{m} a_i N^i + \sum_{j=0}^{n} b_j N^j \qquad (1)$$

Here, P is the pressure expressed in Torr, N is the amount adsorbed in mmol/g, T is thetemperature in K, a_i and b_j are virial coefficients, and m, n represent the number of coefficients required to adequately describe the isotherms (m and n were gradually increased until the contribution of extra added a and b coefficients was deemed to be statistically insignificant towards the overall fit, and the average value of the squared deviations from the experimental values was minimized). The values of the virial coefficients a_0 through a_m were then used to calculate the isosteric heat of adsorption using the following expression.

$$Q_{st} = -R \sum_{i=0}^{m} a_i N^i \qquad (2)$$

Q_{st} is the coverage-dependent isosteric heat of adsorption and R is the universal gas constant. The heat of C_2H_2, C_2H_4, C_2H_6 and CH_4 sorption for activated SNNU-Bai67 in the manuscript are determined by using the sorption data measured in the pressure range from 0-1 bar (273 and 298 K), which is fitted by the virial-equation very well ($R^2 > 0.9999$).

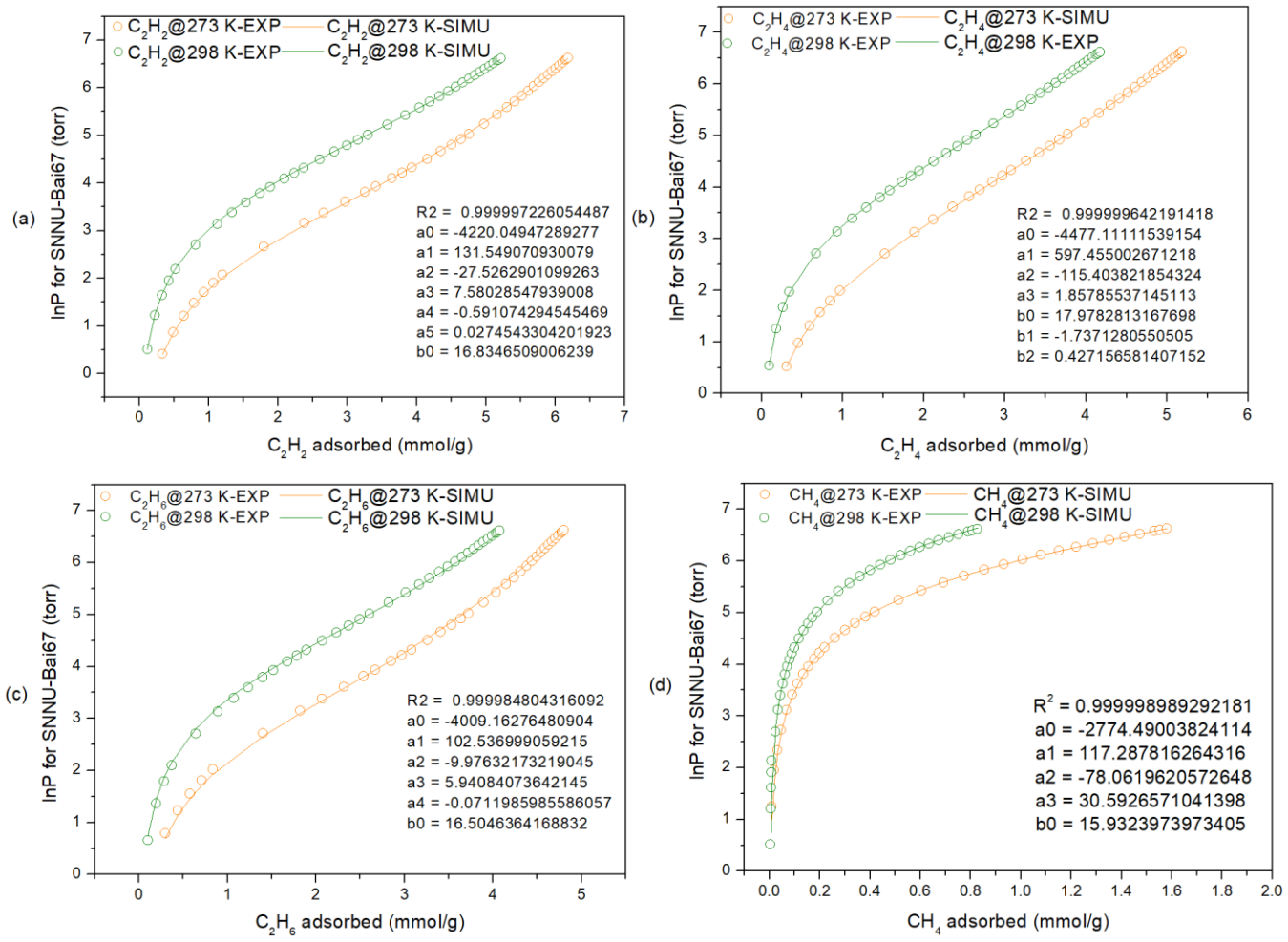

Figure S12. The details of virial equation (solid lines) fitting to the experimental C_2H_2 (a), C_2H_4 (b), C_2H_6 (c) and CH_4 (d) adsorption data (symbols) for activated SNNU-Bai67.

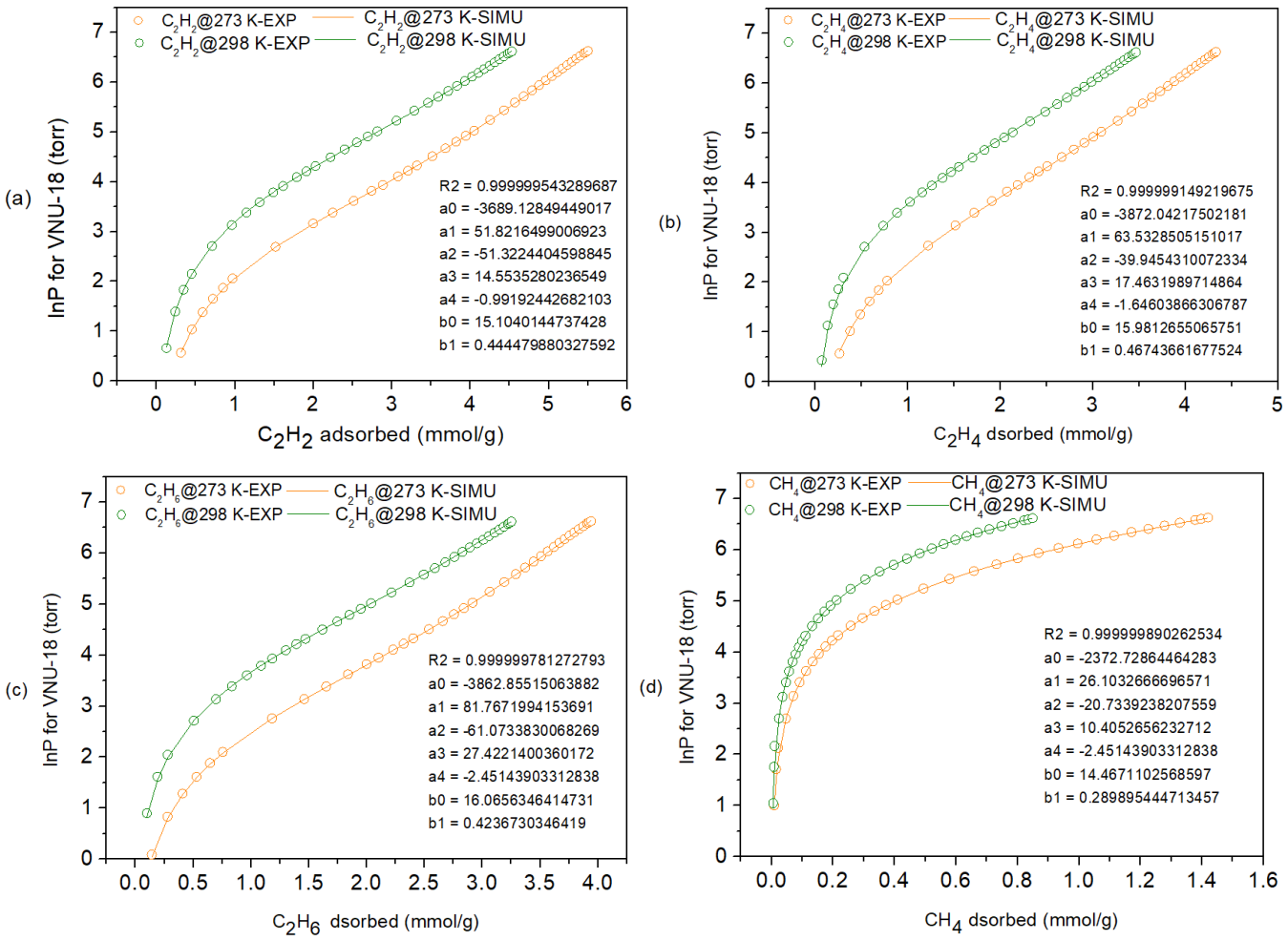

Figure S13. The details of virial equation (solid lines) fitting to the experimental C_2H_2 (a), C_2H_4 (b), C_2H_6 (c) and CH_4 (d) adsorption data (symbols) for VNU-18.

Prediction of the Gas Adsorption Selectivity by IAST. IAST (ideal adsorption solution theory)[5-6] was used to predict binary mixture adsorption from the experimental pure-gas isotherms. In order to perform the integrations required by IAST, the single-component isotherms should be fitted by a proper model. In practice, several methods to do this are available. We found for this set of data that the dual-site Langmuir-Freundlich equation was successful in fitting the data. As can be seen in Figure S14 and Table S2-3, the model fits the isotherms very well ($R^2 > 0.9999$).

$$q = \frac{q_{m,1} b_1 p^{1/n_1}}{1 + b_1 p^{1/n_1}} + \frac{q_{m,2} b_2 p^{1/n_2}}{1 + b_2 p^{1/n_2}} \qquad (3)$$

Here, P is the pressure of the bulk gas at equilibrium with the adsorbed phase (kPa), q is the adsorbed amount per mass of adsorbent (mmol/g), $q_{m,1}$ and $q_{m,2}$ are the saturation capacities of sites 1 and 2 (mmol/g), b_1 and b_2 are the affinity coefficients of sites 1 and 2 (1/kPa), and n_1 and n_2 represent the deviations from an ideal homogeneous surface. The fitted parameters were then used to predict multi-component adsorption with IAST.

The selectivity $S_{A/B}$ in a binary mixture of components A and B is defined as $(x_A/y_A)/(x_B/y_B)$, where x_i and y_i are the mole fractions of component i (i = A, B) in the adsorbed and bulk phases, respectively.

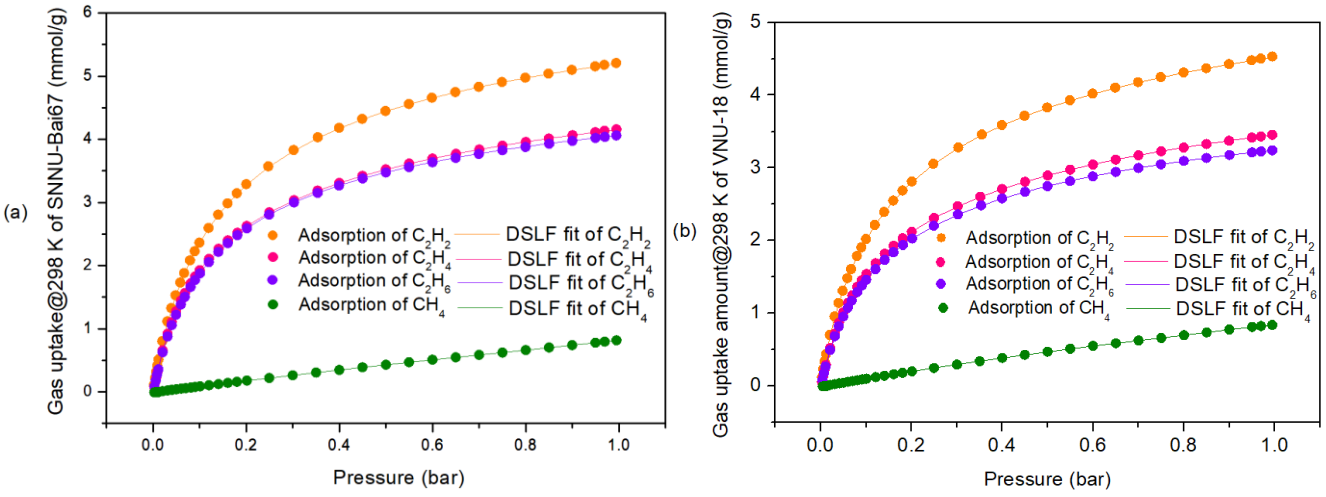

Figure S14. Low pressure gas adsorption isotherms and the dual-site Langmuir-Freundlich (DSLF) fit lines of C_2H_2, C_2H_4, C_2H_6 and CH_4 in SNNU-Bai67 (a) and VNU-18 (b) at 298 K.

Table S2. Dual-site Langmuir-Freundlich parameters for pure C_2H_2, C_2H_4, C_2H_6 and CH_4 isotherms in activated SNNU-Bai67 at 298 K

	SNNU-Bai67			
	C_2H_2	C_2H_4	C_2H_6	CH_4
R^2	0.999993773432604	0.999995326671241	0.999994132308008	0.999977396320602
$q_{m,1}$	2.4928740879393	2.38092409284434	3.06592538141372	7.56767855662538
$q_{m,2}$	4.51534038891507	3.36971559425661	2.35228182283931	0.0175596152872175
b_1	0.0151093385937918	0.134412427645968	0.110691078400833	0.00140410425964977
b_2	0.0995645778573002	0.0232484590714453	0.018552762173548	4.85724902534828E-35
n_1	1.111736252	0.946400212	1.013563138	1.033635678742880
n_2	1.060512841	1.141609791	1.109310821	0.057455926122578

Table S3. Dual-site Langmuir-Freundlich parameters for pure C_2H_2, C_2H_4, C_2H_6 and CH_4 isotherms in VNU-18 at 298 K

	VNU-18			
	C_2H_2	C_2H_4	C_2H_6	CH_4
R^2	0.999997566124258	0.999995165406282	0.999993077253106	0.999982088511563
$q_{m,1}$	2.48311044977533	2.12175878108389	2.45563781206927	0.0165938504076144
$q_{m,2}$	4.256599107818	2.8448595637287	2.02866315054155	3.24870054992584
b_1	0.00929287161151276	0.123538219446429	0.110469936023112	1.45102717371289E-54
b_2	0.0971281133138944	0.0194245812009864	0.0161451009227828	0.00347104908037213
n_1	1.138639412	0.988141097	1.03472122	0.035892711009700
n_2	1.105931607	1.140459065	1.105922555	1.000375151588010

Computation Detail. Atomistic GCMC simulations were performed to estimate the adsorption isotherms of C_2H_2, C_2H_4, C_2H_6 and CH_4 in SNNU-Bai67 and VNU-18. The framework of SNNU-Bai67 and VNU-18 were fixed from their crystallographic data. All simulations/calculations were performed by the Materials Studio 7.0 package. DFT and PDFT calculations were performed by the Dmol3 module, using the generalized gradient approximation (GGA) with the Perdew-Burke-Ernzerhof (PBE) functional and the double numerical plus d-functions (DNP) basis set, TS for DFT-D correction, and the Effective Core Potentials (ECP).[7,8] The Mulliken charges of the atoms of the framework were calculated by PDFT performed through the Dmol3 module. The C_2H_2, C_2H_4, C_2H_6 and CH_4 gas molecules were optimized using the DMol3 method and adopted the B3LYP fitted ESP-charge.[9] The adsorption isotherms of C_2H_2, C_2H_4, C_2H_6 and CH_4 gases at 298 K were estimated through Grand Canonical Monte Carlo (GCMC) simulations by using the adsorption isotherm task and metropolis method in the sorption calculation module.[6,7] Both the framework and gas molecule were regarded as rigid. The equilibration steps and production steps were set to 1×10^6 and 1×10^7, respectively. The framework and gas molecule were described by the COMPASSII. The cutoff distance was set to 18.5 Å for the Lennard-Jones (LJ) interactions, and the electrostatic interactions and the van der Waals interactions were handled using the Ewald and Atom based summation method, respectively. The adsorption locations of C_2H_2, C_2H_4, C_2H_6 and CH_4 molecules were searched through Grand Canonical Monte Carlo (GCMC) simulations by using the location task and metropolis method in the sorption calculation module. The loading steps, production steps and temperature cycles were set to 1×10^5, 1×10^7 and 40, respectively.

The adsorption isotherms for C_2H_2, C_2H_4, C_2H_6 and CH_4 gases of SNNU-Bai67 and VNU-18 were simulated at 298 K and below 1 bar. As shown in Fig. S16, the adsorption uptakes for C_2H_2, C_2H_4, C_2H_6 and CH_4 of SNNU-Bai67 and VNU-18 were both overestimated, which could be due to the fact that a perfect crystal is utilized in simulation or inaccuracies in the present simulation model. However, for SNNU-Bai67, the trend of adsorption uptakes over the whole pressure range is C_2H_2>C_2H_4>C_2H_6>CH_4, with those of C_2H_4 and C_2H_6 being similar and VNU-18 exhibits the similar trend of those adsorption uptakes, both of which are consistent with those observed in experimentally, respectively. Moreover, the adsorption uptakes for C_2H_2, C_2H_4 and C_2H_6 of SNNU-Bai67 are slightly higher than those of VNU-18, respectively and that for CH_4 of SNNU-Bai67 is similar to the value of VNU-18, which is also consistent with those observed experimentally, respectively.

The adsorption locations of C_2H_2, C_2H_4, C_2H_6 and CH_4 molecules in SNNU-Bai67 and VNU-18 were searched with their adsorption uptakes being equal to those measured in experiments at 1 bar, as shown in Fig. 5. In SNNU-Bai67, the C_2H_2, C_2H_4 and CH_4 molecules with numbers of 13, 10 and 2, respectively, within one unit are all located at the square units in the partial corn-sql layer, whereas 9 of C_2H_6 molecules

are located at the square units in the partial corn-sql layer and another one C_2H_6 molecule occupies the corner of pillars. In comparison, in VNU-18, the C_2H_4 and CH_4 molecules with numbers of 8 and 2, respectively, within one unit are all located at the square units in the partial corn-sql layer, whereas 9 of C_2H_2 and 7 of C_2H_6 molecules are located at the square units in the partial corn-sql layer and another two C_2H_2 molecules and one C_2H_6 molecule occupies the corner of pillars.

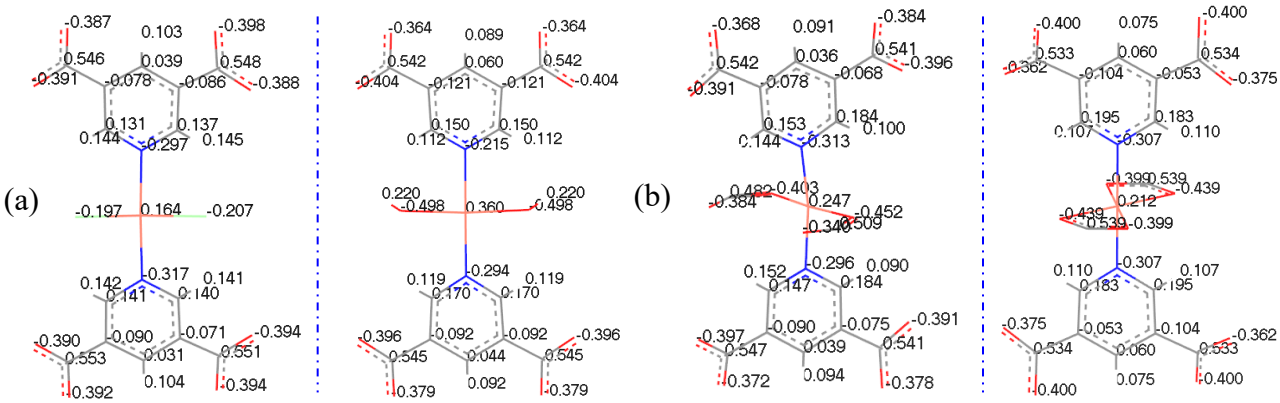

Figure S15. The ESP charges used in the GCMC simulations for atoms of ligands constituting the partial corn-*sql* layers in SNNU-Bai67 and VNU-18.

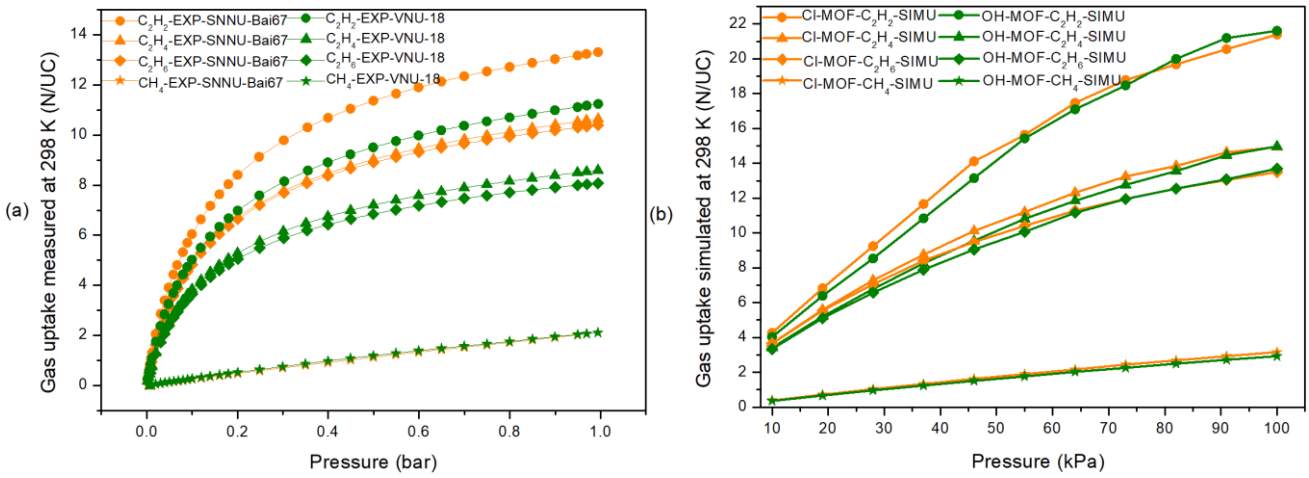

Figure S16. The experimental (a) and simulated (b) C_2H_2, C_2H_4, C_2H_6 and CH_4 adsorption isotherms for SNNU-Bai67 and VNU-18 at 298 K with the unit of gas uptake as N/UC.

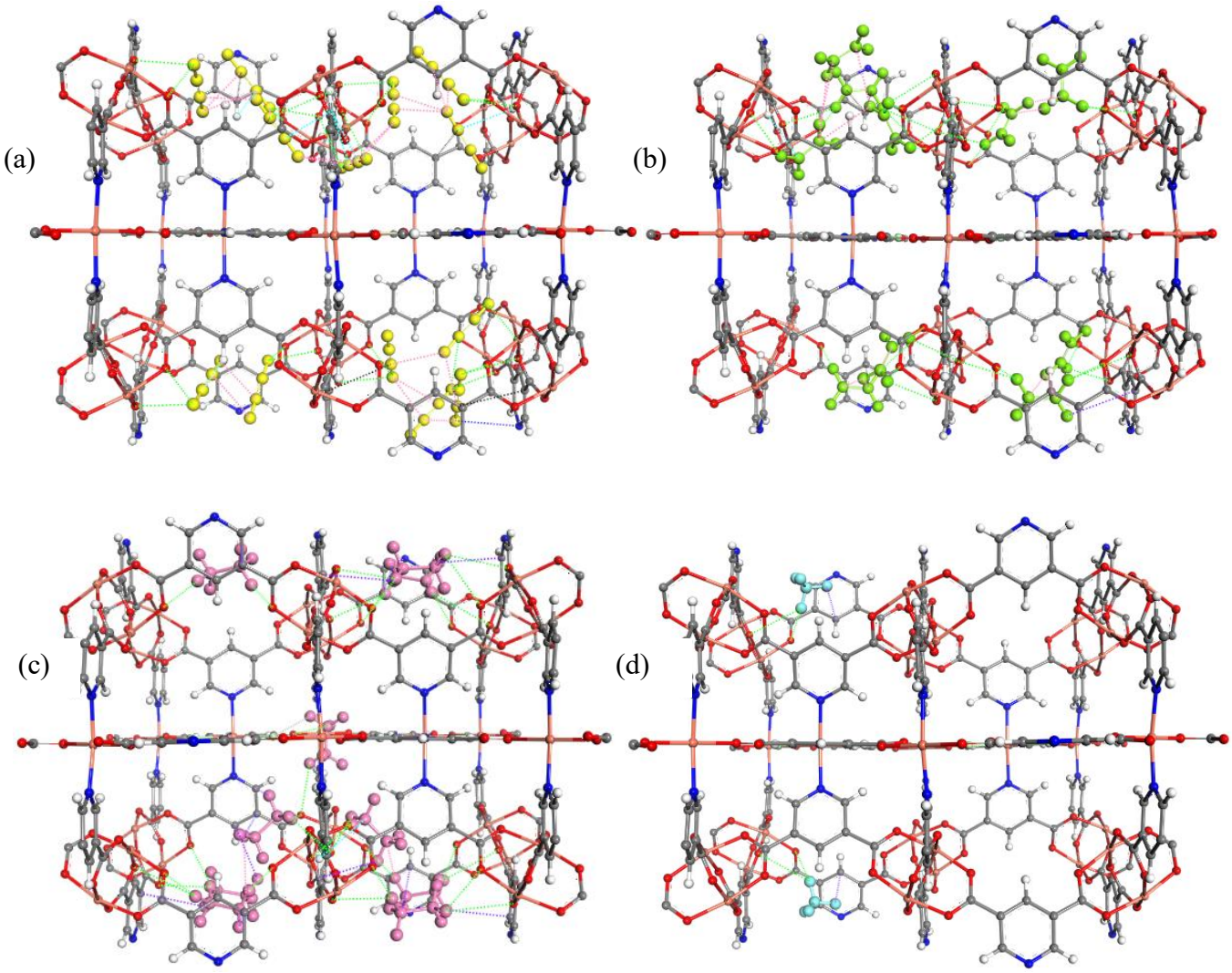

Figure S17. The interactions of H_{C2H2}…O_{COO} (green), H_{C2H2}…N_{Py} (blue), H_{Py}…C_{C2H2} (turquiose), π…π (black) and H_{C2H2}…C_{C2H2} (pink) in SNNU-Bai67 (a); the interactions of H_{C2H4}…O_{COO} (green), H_{C2H4}…C_{Py} (purple), H_{Py}…C_{C2H4} (turquiose), π…π (black) and H_{C2H4}…C_{C2H4} (pink) in SNNU-Bai67 (b); the interactions of H_{C2H6}…O_{COO} (green), H_{C2H6}…C_{Py} (purple), H_{Py}…C_{C2H6} (turquiose), H_{C2H6}…Cl^- (grey) and H_{C2H6}…C_{C2H6} (pink) in SNNU-Bai67 (c); the interactions of H_{CH4}…O_{COO} (green) and H_{CH4}…C_{Py} (purple) in SNNU-Bai67 (d).

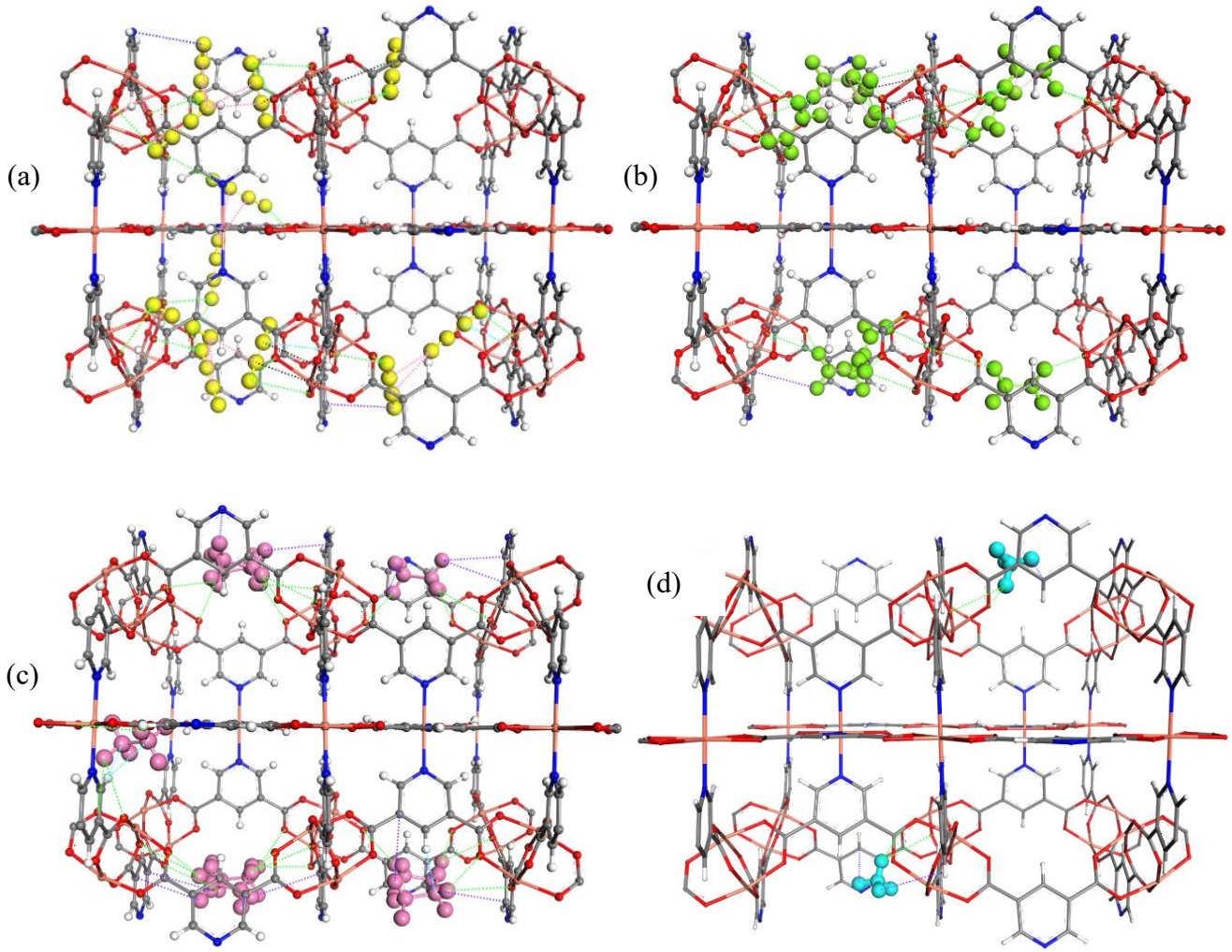

Figure S18. The interactions of H_{C2H2}…O_{COO} (green), H_{C2H2}…N_{Py} (blue), H_{C2H2}…C_{Py} (purple), H_{Py}…C_{C2H2} (turquiose), π…π (black) and H_{C2H2}…C_{C2H2} (pink) in VNU-18 (a); the interactions of H_{C2H4}…O_{COO} (green), H_{C2H4}…C_{Py} (purple), π…π (black) and H_{C2H4}…C_{C2H4} (pink) in VNU-18 (b); the interactions of H_{C2H6}…O_{COO} (green), H_{C2H6}…C_{Py} (purple), H_{C2H6}…N_{Py} (blue), H_{Py}…C_{C2H6} (turquiose), and H_{C2H6}…C_{C2H6} (pink) in VNU-18 (c); the interactions of H_{CH4}…O_{COO} (green) and H_{CH4}…C_{Py} (purple) in VNU-18 (d).

Reference

[1] G. M. Sheldrick, *Acta Crystallogr. Sect. A*, 2008, **64**, 112.

[2] A. L. Spek, *J. Appl. Crystallogr.*, 2003, **36**, 7.

[3] a) K. S. Walton and K. S. Snurr, *J. Am. Chem. Soc.*, 2007, **129**, 8552; b) J. Rouquerol, P. Llewellyn and F. Rouquerol, *Stud. Surf. Sci. Catal.*, 2007, **160**, 49.

[4] J. L. C. Rowsell, O. M. Yaghi, *J. Am. Chem. Soc.* 2006, **128**, 1304.

[5] A. L. Myers, J. M. Prausnitz, *AIChE J.* 1965, **11**, 121.

[6] a) Y. S. Bae, K. L. Mulfort, H. Frost, P. Ryan, S. Punnathanam, L. J. Broadbelt, J. T. Hupp, R. Q. Snurr, *Langmuir* 2008, **24**, 8592; b) B. Mu, F. Li, K. S. Walton, *Chem. Commun.* 2009, 2493.

[7] P.-Q. Liao, N.-Y. Huang, W.-X. Zhang, J.-P. Zhang and X.-M. Chen, *Science*, 2017, **356**, 1193.

[8] Y. Wang, N.-Y. Huang, J.-Q. Shen, P.-Q. Liao, X.-M. Chen and J.-P. Zhang, *J. Am. Chem. Soc.*, 2018, **140**, 38-41.

[9] H.-G. Hao, Y.-F. Zhao, D.-M. Chen, J.-M. Yu, K. Tan, S. Ma, Y. Chabal, Z.-M. Zhang, J.-M. Dou, Z.-H. Xiao, G. Day, H.-C. Zhou and T.-B. Lu, *Angew. Chem. Int. Ed.*, 2018, **57**, 16067-16071.